nature communications

Article

https://doi.org/10.1038/s41467-026-69533-7

Spectroscopic limits of diamond anvils to 520 GPa and projected bandgap closure

Received: 12 September 2025

Accepted: 30 January 2026

Published online: 12 February 2026

Check for updates

A. Hilberer[1,2] ✉, P. Loubeyre[1,2] ✉, C. Pépin[1,2], F. Occelli[1,2], G. Weck[1,2], R. André[1,2] & P. Dumas[1,3]

Diamond anvils serve as optical windows in static ultrahigh-pressure experiments, now reaching the terapascal regime. However, they exhibit poorly understood changes in their optical properties under multimegabar pressure. Here, we present broadband absorption measurements (ultraviolet to infrared wavelengths) up to 520 GPa, revealing a pronounced loss of transparency with pressure. Diamond Raman scattering is used to infer the stress profile along the anvils' axis under the assumption of tetragonal distortion, and crucially at the sample interface. This enables a quantitative analysis of absorption spectra, showing an indirect bandgap narrowing towards the infrared, with metallization projected near 560 GPa sample pressure within our stress model. A universal optical behavior is observed across different anvil geometries, which is consistent with the universality of the Raman edge pressure scale, here refined. These findings help define the spectroscopic operational limits of diamond anvil cells under extreme pressure with important implications for recent claims of hydrogen metallization.

The Diamond Anvil Cell (DAC) is a workhorse of static high-pressure physics. It fully exploits the exceptional mechanical properties of diamond—namely its record-breaking hardness, ability to undergo significant elastic deformation, and remarkable optical transparency due to a wide indirect bandgap. A wide range of spectroscopic techniques have been adapted to probe the properties of materials under high pressure[1], with one of the latest developments being magnetic measurements using NV quantum sensors (ref. 2 and references therein). A wealth of data on material properties at high pressures have been obtained up to the conventional DAC limit of about 400 GPa[3]. Currently, the frontier of extreme pressure research lies in the terapascal (TPa) regime. This range is readily accessible through shockless dynamic compression techniques available at large laser facilities[4,5]; however, microscopic diagnostics under such approach are typically limited to X-ray diffraction. Static compression into the TPa regime has been made possible by two novel anvil designs: toroidal anvils and the double-stage anvil, which have reached pressures close to 600 GPa[6] and 1000 GPa[7], respectively. The toroidal DAC, in particular, offers advantages in terms of sample volume and optical access, enabling continued use of spectroscopy probes up to ultrahigh pressures.

Among the key motivations for reaching pressures in the 0.5–1 TPa range is the quest to reach the atomic metallic state of hydrogen. This phase is predicted to exhibit many intriguing quantum phenomena, such as room-temperature superconductivity[8], supersolidity[9], or a combined superfluid-superconducting state[10]. Various claims of observation have been made regarding metallic hydrogen, including a semi-metallic state near 350 GPa[11], molecular metallic hydrogen at around 425 GPa for H_2[12] and 460 GPa for D_2[13], and atomic metallic hydrogen near 500 GPa[14]. However, these findings are not fully consistent, and the claim of atomic metallic hydrogen has faced serious criticism[15]. Central to the debate are two key issues: the differences in the diamond Raman edge-based pressure scales used[16,17], and the pressure-induced changes in the optical properties of stressed diamond. Recently, the Raman pressure scale has been recalibrated up to 0.5 TPa, demonstrating its robustness across different anvil geometries. Using only this refined pressure scale has helped to improve consistency in literature hydrogen Raman data[18]. Yet, the effect of

[1]CEA DAM DIF, Arpajon, France. [2]Laboratoire Matière en Conditions Extrêmes, Université Paris-Saclay, CEA, Bruyères-le-Châtel, France. [3]Synchrotron SOLEIL, Gif-sur-Yvette, France. ✉e-mail: antoine.hilberer@cea.fr; paul.loubeyre@cea.fr

diamond transparency remains to be studied to critically evaluate the metallization claims.

Since the 1990's, it has been recognized that deviatoric stresses at the anvil tip significantly affect the optical properties of the diamond window[19,20]. Specifically, the absorption edge of diamond has been observed to shift to lower energies with increasing pressure. Ab initio calculations suggested that diamond's minimum bandgap is highly sensitive to anisotropic stress, and that beyond a certain level of tetragonal distortion, the bandgap decreases with pressure—opposite to what occurs under hydrostatic compression[21–23]. However, this loss of transparency under extreme pressure has remained a qualitative observation. Progress toward a quantitative understanding demands to consider several issues: the non-uniform stress distribution within the anvil, evolution of deviatoric stress with pressure, dependence on anvil geometry and difficulty to reach pressures in excess of 300 GPa. This is tackled here below using optical absorption spectroscopy experiments performed in DACs, allowing for the quantitative extraction of the pressure evolution of the indirect bandgap in diamond under proposed tetragonal distortion, corresponding to the maximally stressed layer of diamond at the sample interface. Based on these findings, the pressure limits for various spectroscopic techniques, commonly used to characterize samples under very high pressure in a DAC, are discussed.

Results

Marked visual changes in diamond anvils above 300 GPa

The main effect is illustrated in Fig. 1A, which shows a complete loss of transparency in the visible range around 500 GPa. We have measured the optical transmission spectra of diamond anvils from the UV to near-infrared (220–950 nm) range with increasing pressure. Two complementary setups were used: one using the SOLEIL synchrotron as a UV source, and the other one using a supercontinuum laser (see Supplementary Fig. 2). Experiments were performed using different anvil shapes oriented with the [100] diamond axis on the compression direction, beveled and toroidal geometries, and all diamond anvils were electronic-grade type IIas, so as to minimize any influence of impurities. All DACs were loaded with a neon sample, as solid neon remains a wide bandgap insulator into the TPa range[24] so any

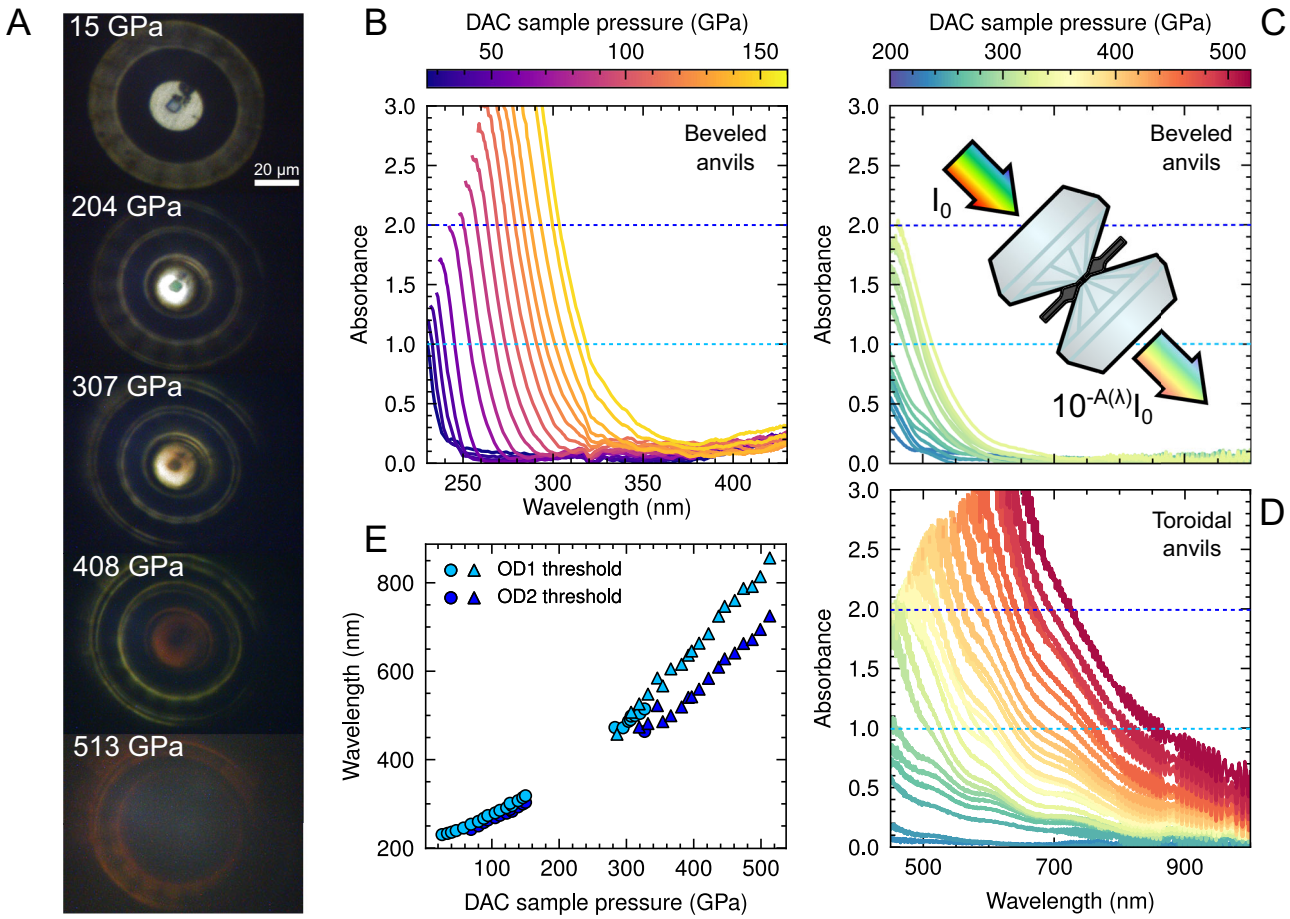

Fig. 1 | Evolution of the transparency of diamond anvils under extreme pressure. A Visible microscopy images of a Ne sample confined in a DAC with toroidal diamond anvils, at pressures from 15 GPa to over 500 GPa. The toroidal shape of the diamond tip modifies the usual appearance of a standard DAC sample. The central bright area corresponds to the 24 μm culet of the toroidal diamond anvil, while the small gray disk near its center is the gasket hole (~4 μm in diameter) that contains the neon sample. The dark spots on the upper-right edge of the culet correspond to fluorescence pressure gauge particles, used as pressure markers during pre-indentation of the gasket. The dark region surrounding the culet is caused by the toroidal groove. More details about sample geometry are shown in Supplementary Fig. 1. Diamond intrinsic pressure-induced absorption from the closing bandgap is visible in the red color and eventual opacity acquired by anvils with increasing pressure. All three presented samples reaching above 300 GPa showed this effect in visible-light images. **B** UV absorbance data collected through a DAC loaded with a neon sample from 26 to 139 GPa, with 70 μm culet beveled anvils. **C** VIS-NIR absorbance data collected through a DAC loaded with a neon sample from 220 to 328 GPa, with 20 μm culet beveled anvils. **D** VIS-NIR absorbance data collected through a DAC loaded with a neon sample from 234 to 513 GPa, with 24 μm culet toroidal anvils. **E** Measured wavelengths for Optical Density (OD) values of 1 and 2 as a function of sample pressure. The apparent data gap between 160 GPa and 280 GPa is thus due to the difference between the highest pressure achieved in UV spectroscopy experiment, and the lowest pressure at which absorbance could be detected in visible-IR experiments. Round symbols are data from beveled anvils, triangles are from toroidal anvils.

absorption from the Ne sample could be neglected. The evolution of the observed diamond absorption edge from ambient pressure to over 500 GPa is shown in Fig. 1B–D, corresponding to three independent runs, each targeting a different pressure range with specific anvils. A continuous redshift of the absorption edge is observed. This shift is quantified in Fig. 1E, which reports optical density thresholds of 1 and 2 under pressure. This evolution was found reversible with pressure cycling and reproducible across different runs (see Supplementary Fig. 11). While absorption spectroscopy is a well-established technique for determining the bandgap of a semiconductor, its use in the present case is more complex. The absorption of light is not measured through a homogeneous sample, but rather along the entire axis of the diamond anvils, where the tensorial stress continuously evolves from ambient hydrostatic pressure to the maximum pressure at the sample interface, accompanied by a large elastic tetragonal distortion of the diamond lattice. Understanding this internal stress distribution is therefore essential for accurately interpreting the absorption data.

Stress state in the diamond anvil tip inferred from Raman measurements

Under [100] axial pressure loading, only the diamond Raman singlet LO mode is observed in back-scattering geometry. The shift of this phonon mode, derived from the Raman edge spectra, has been calibrated as a pressure gauge for multi-megabar pressures[16]. Above 300 GPa, the calibration validity could be questioned, as it relies on an inaccurate equation of state (EOS) of platinum[17]. A recent calibration resolved this issue and aligns well with the extrapolation of the calibration made up to 300 GPa[18]. Also, a key finding of that study is the robustness of the diamond edge scale to variation in the load distribution and to operation with diamond anvils of different shapes. In the present work, we conducted a similar calibration using gold samples as the X-ray pressure standard. Measurements of the phonon edge frequency versus pressure, conducted with both toroidal and beveled anvils, follow a single curve (Fig. 2), confirming the universal applicability of the Raman diamond edge scale. Furthermore, the fit shows

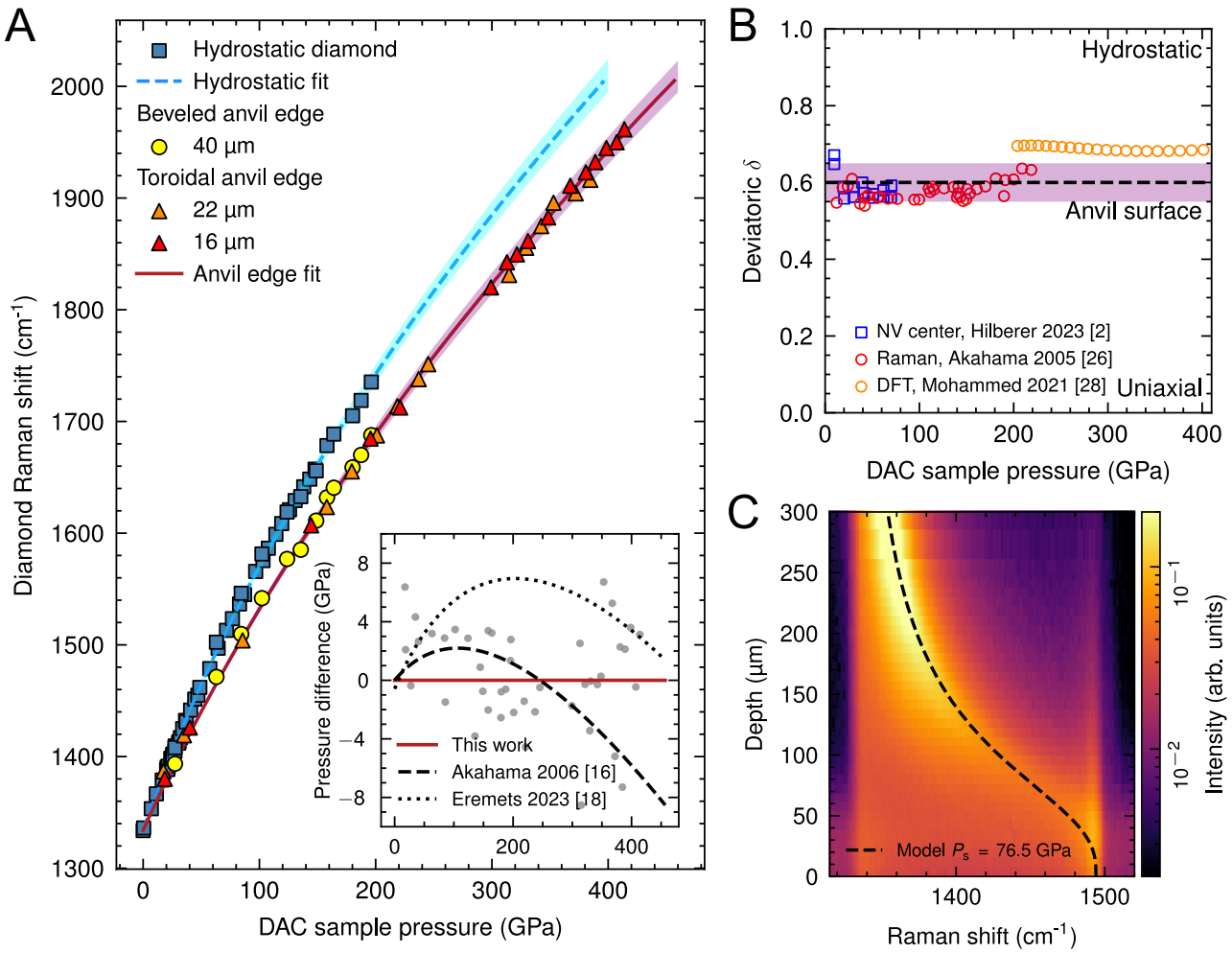

Fig. 2 | Diamond Raman egde scale. A Pressure dependence of the first order Raman mode of diamond. Blue squares show the peak Raman shift of the three-fold degenerate T_{2g} diamond mode under hydrostatic pressure. Red, orange and yellow symbols correspond to the diamond anvil high-frequency Raman edge. Pressure was measured by simultaneous X-ray diffraction of gold samples corrected for the IPPS-Ruby2020 recommended EOS[25]. Fits to the data using the standard equation $P = K_0 \frac{\Delta\nu}{\nu_0}(1 + \frac{1}{2}(K'_0 - 1)\frac{\Delta\nu}{\nu_0})$ from ref. 16 yield parameters $K_0 = 443 \pm 5$ GPa and $K'_0 = 4.1 \pm 0.1$ for hydrostatic compression, $K_0 = 575 \pm 7$ GPa and $K'_0 = 3.3 \pm 0.1$ for the anvil edge. Shaded error bands show one standard deviation errors on the fit parameters. Ambient pressure diamond Raman shift is set to $\nu_0 = 1334$ cm^{-1}. The inset shows the difference in pressure estimation between the pressure scale from the fit to our data and previously published work[16,18]. Gray points are residuals from our data compared to our fit. **B** Estimates for the stress anisotropy parameter δ at the diamond anvil surface (stress in the plane of the culet is δP_s where P_s is sample pressure) from refs. 2,26,28. The value selected for further analysis here is the mean of all these values, denoted by the dashed line, with error taken as their standard deviation shown by the purple-shaded region (0.6 ± 0.05). **C** Colormap of the intensity of the diamond Raman signal collected at varying depths relative to the loaded surface of a beveled anvil at a sample pressure of 77 GPa. The black dashed line represents the pressure profile predicted by a simple stress model (described in "Methods").

excellent agreement with the recent calibration. Minor discrepancies are attributed to differences in the gold EOS since we updated the gold EOS to align with the IPPS-Ruby2020 scale[25] (see Supplementary Fig. 7). The Raman phonon was also measured under hydrostatic compression of diamond, in which case the triply degenerate LO-TO mode is observed, thereby extending previous data to 200 GPa. The difference in Raman frequency between the hydrostatic and the anvil-tip cases arises from anisotropic stress in the latter. Stress normal to the diamond surface at the anvil culet center can be taken as the sample pressure, P_s, and the stress tensor assumed to have axial symmetry with a perpendicular proportional component δP_s. Raman data were used to reconstruct the stress state at diamond tip using recent ab initio calculations of the diamond Raman frequencies under non-hydrostatic stress[26]. Notably, it is found that the deviatoric stress parameter δ remains nearly constant under pressure, around 0.68. Linear elasticity calculations predicts δ = 0.61[27], while NV centers measurements determined δ = 0.57 to be constant up to at least 70 GPa[2]. In the case of [111]-oriented anvils, the splitting of LO/TO phonon modes can be measured by Raman spectroscopy and the deviatoric ratio can be estimated, as reported up to 220 GPa[28]. In this configuration, the deviatoric ratio was found to remain constant at 0.56 up to about 100 GPa, in very good agreement with NV measurements under [100] loading. Above 100 GPa, it may gradually increase with a weak pressure dependence, reaching only 0.63 at 220 GPa. These independent estimates, summarized in Fig. 2B, give further confidence that δ can be considered constant with sample pressure, about 0.6 ± 0.05 in our analysis. The axial pressure distribution along the diamond anvil axis was mapped using confocal Raman spectroscopy. As shown in Fig. 2C, the observed pressure evolution along the compression axis is well reproduced by a simplified elasticity model of a semi-infinite anvil with uniform pressure applied to a circular flat face[29]. A notable feature of this pressure evolution is the presence of a region with nearly constant pressure extending a few microns below the culet surface, followed by a quasi-exponential pressure decrease with increasing depth. The thickness of this uniform slab is mostly determined by the diameter of the loaded region, i.e., the anvil culet (see "Methods"). Recently, the pressure distribution within a diamond anvil was studied using spatially-resolved inelastic X-ray scattering, however only a monotonous pressure decay was observed, and the constant stress layer could not be resolved[30]. Still, this study confirmed the fast pressure decay within the anvil thickness, supporting the idea that the absorption edge of stressed anvils along their axis should be dominated by the high pressure layer close to the tips.

Our Raman study thus supports the existence of a homogeneous, tetragonally distorted diamond slab—several microns thick—located at the center of the anvil tip/sample interface, where the axial pressure distribution within the anvil reaches its maximum and the deviatoric stress parameter remains constant up to the highest pressures reached. This configuration is favorable for extracting the pressure dependence of the bandgap in the tetragonally distorted diamond from absorption data.

Determination of the indirect bandgap energy from absorption data

One of the most fundamental properties affecting the optical behavior of diamond is the bandgap describing the energy barrier between conduction and valence bands. Absorption measurements were first used in the 1960's to determine the energy value of the indirect bandgap in diamond, found to be 5.47 eV under ambient conditions[31]. Redshift and blueshift of this bandgap were also measured by absorption, under increasing temperature[32] and pressure[22,23,33]. For diamond, optical absorption spectroscopy primarily probes the indirect bandgap, with indirect inter-band transitions assisted by phonons dominating the absorption process near the threshold. As a result, the absorption coefficient above the absorption threshold is described as being proportional to $(h\nu \pm E_{ph} - E_g)^2$, where $h\nu$ is the photon energy, E_{ph} is the phonon energy and E_g is the indirect bandgap energy. The $\pm E_{ph}$ accounts for phonon absorption and emission processes, both of which occur at 300 K. Using the LO phonon energy as given in Fig. 2, the phonon contribution is estimated to be at most 0.25 eV in the 300 GPa range. In our analysis, we neglect this contribution, as the induced error falls within the uncertainty of the current bandgap determination. In Fig. 3A, we apply the standard method for extracting the indirect bandgap value from the absorption threshold by plotting $A^{1/2}$ versus $h\nu$, where A is the absorbance defined as $-\log(I/I_0)$. A clear linear region at the threshold is observed, consistent with previous absorption studies, and the indirect bandgap E_g is thus determined from the x-intercept of this linear region. These results can be explained within our stress model by the presence of a homogeneous diamond slab—located at the diamond–sample interface—that dominates the absorption threshold. Indeed, the measured absorption spectra are well reproduced by the model (discussed further in "Methods") that incorporates the stress distribution in the diamond anvil tip, consistent with Raman measurements. This agreement is illustrated in Fig. 3B, where the absorbance spectra calculated at 80 GPa and 328 GPa closely match observations.

This analysis proves effective for beveled anvils, while in the case of toroidal anvils the absorption threshold appears more broadened in energy. This likely indicates that the homogeneous layer at maximum pressure at the sample interface is not sufficiently thick to dominate the absorption threshold in this geometry. Nevertheless, the evolution of the OD = 1 threshold with pressure—which tracks the minimum bandgap, albeit shifted in pressure—agrees between beveled and toroidal anvils (see Fig. 3C). This consistency supports a universal evolution of diamond anvil minimal bandgap, that is independent of tip geometry similarly to the behavior observed for the diamond Raman edge scale.

At the diamond anvil's tip, the bandgap decreases with pressure, as expected for diamond subjected to tetragonal distortion under anisotropic stress. Considering that this evolution occurs under a quasi-constant deviatoric stress parameter $\delta = 0.6 \pm 0.05$, the average pressure in the maximally distorted diamond slab is given by $P = P_s(1 + 2\delta)/3$, P_s being the quasi-hydrostatic sample pressure in contact with the diamond anvil. The measured evolution of the indirect bandgap is converted to a density dependence, within our anisotropic stress model, using diamond's EOS (IPPS-Ruby2020[25] recommended values, see "Methods") and the mean pressure, as shown in Fig. 3C. A linear relationship between the indirect bandgap and density is observed. Extrapolation of this trend suggests that the indirect bandgap would close at an estimated density of 5.41 ± 0.05 g/cm^3, corresponding to a sample pressure of about 555 ± 6 GPa. Sample pressures about 600 GPa have been reported using toroidal anvils[6] and diamond was not observed to lose its strength, even though metallization may have occurred in the thin diamond layer in contact with the sample.

Spectroscopic limitations illustrated in the search for metallic hydrogen

Up to now, only light absorption and scattering techniques have been implemented to probe the properties of matter in the DAC above 400 GPa. The primary diagnostics rely on high-brilliance hard X-ray beams (>15 keV) produced at large-scale facilities[34]. The X-ray transparency of the diamond anvils is not affected by the closure of their indirect bandgap, and measurements in the TPa range should be performed similarly to those at a few GPa, especially since X-ray beams can now be focused to sub-micron spots. In our case, X-ray diffraction of the Ne sample and the Re gasket was used on our highest pressure run to determine the sample pressure at 523 ± 13 GPa (Supplementary Fig. 12), at which point Raman edge determination was no longer possible due to diamond absorption. This pressure measurement

https://doi.org/10.1038/s41467-026-69533-7

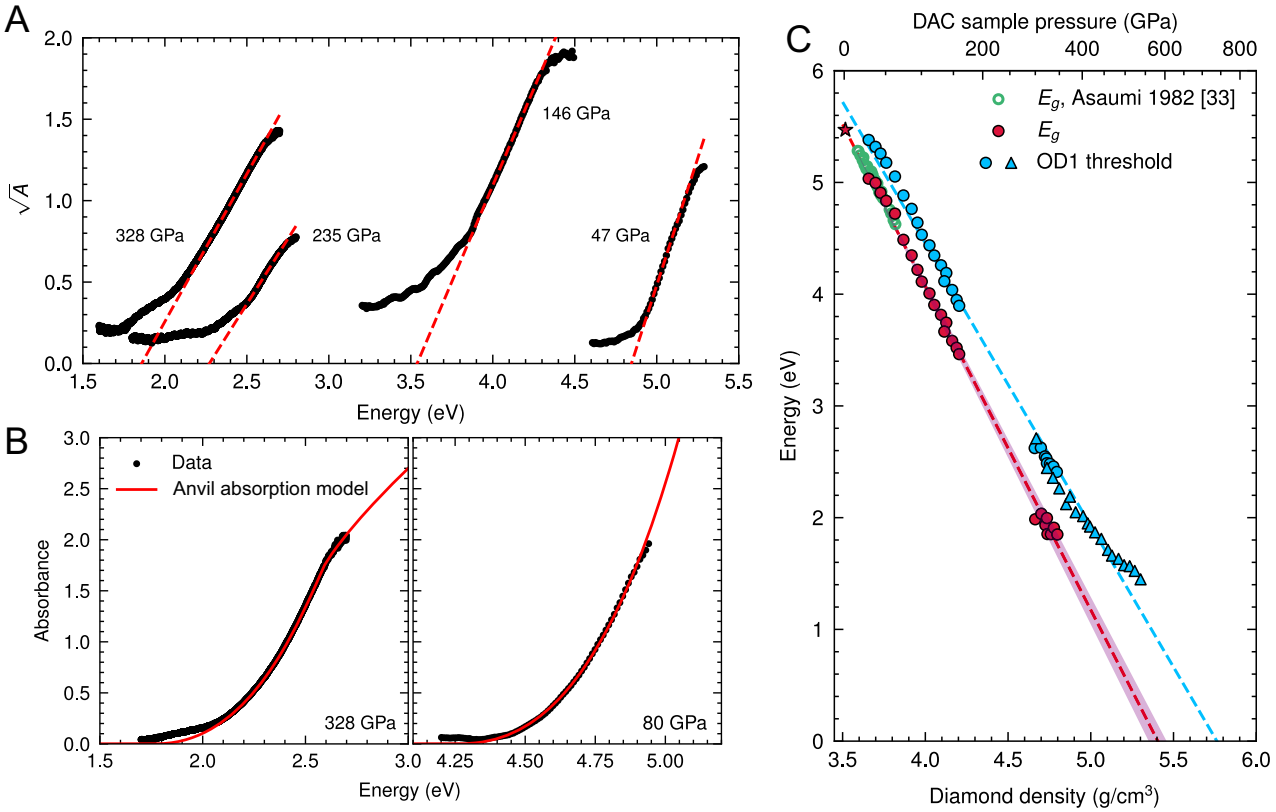

Fig. 3 | Diamond anvil bandgap estimation with applied stress. A Square root of four typical measured diamond anvil absorbance curves at various pressures. The linear portion is fitted to extract minimal bandgap E_g estimates (red dashed lines). All measured curves are shown in Supplementary Fig. 4. **B** Diamond anvil absorbance curves at 80 and 328 GPa, with corresponding estimates from an absorption model taking into account the contributions from the stress gradient along the anvil axis (see "Methods"). **C** Extracted values for the diamond anvil minimum indirect bandgap E_g as a function of diamond density at the anvil tip (estimated for the average pressure $P = P_s(1+2\delta)/3$). The observed density-linear dependencies are fitted by the dashed lines. The purple shaded area denotes one standard deviation error for the fit including error on δ, as well as diamond EOS uncertainties. The red star indicates the diamond bandgap value constraint at ambient pressure. Round symbols are data from beveled anvils, triangles are from toroidal anvils. Data up to 55 GPa from ref. 33 are reported for comparison.

aligns well with the evolution of sample pressure versus applied force on the piston (Supplementary Fig. 9). Additionally, X-ray absorption mapping across the sample clearly reveals the positions of the gasket and Ne sample (Fig. 4) and enables measurement of the thickness profile across the sample chamber. Unfortunately, X-ray diffraction on hydrogen samples remains extremely challenging, and the maximum achieved pressure—about 250 GPa—is still well below the predicted metallization pressure[35].

In laboratory high-pressure experiments, Raman scattering and optical absorption are the two most widely used optical spectroscopy techniques. Both are affected by pressure-evolution of the indirect bandgap, which governs the transparency of diamond. The measured changes in diamond anvil transparency with pressure define three pressure-energy regimes (as shown in Fig. 4): one in which optical measurements are unaffected, one where they are partially perturbed between the indirect bandgap and an optical density threshold of 2, and one where measurements become impossible. This evolution of transparency with pressure applies similarly to measurements in reflection, due to the dual light path through one anvil in this configuration. This classification is exemplified in the present Ne measurements. Above 480 GPa, the Ne sample becomes completely obscured by the anvils (Fig. 4C), marking the onset of the opaque-anvil regime in the visible spectrum. However, the sample remains observable in the infrared using wavelengths around 1900 nm, which is only slightly absorbed even at 520 GPa. Conversely, Raman diamond edge measurements become infeasible above 480 GPa (Supplementary Fig. 10), as the 660 nm excitation line we used reaches the OD = 2 threshold. Pressures beyond this point were extrapolated from the pressure vs load curve (Supplementary Fig. 9) and subsequently validated by X-ray diffraction, as mentioned previously.

The observation of metallic hydrogen has recently been reported by two groups. Both used the Raman pressure scale of ref. 16, which differs only slightly from the present updated calibration, thereby supporting the accuracy of their reported pressures. The first group employed infrared absorption and reported a probable transition to the molecular metallic state at 425 GPa for hydrogen[12] and 460 GPa for deuterium[13]. As shown in Fig. 4, these infrared measurements fall within the transparent diamond anvil regime and thus do not require reevaluation. The second group claimed the observation of atomic metallic hydrogen at 495 GPa[14], based on visual inspection in the visible range and reflectance measurements at four wavelengths (three visible and one near-infrared). However, as shown in Fig. 4, both visual observation and reflectance in the visible fall deep within the opaque anvil regime at this claimed pressure. Only the near-infrared reflectance point could remain accessible, though still significantly affected by anvil absorption. This inconsistency with the now well-established pressure-dependent transparency of diamond anvils raises serious doubts about the validity of the claim and quantitatively reinforces earlier criticisms[36,37]. As such, the observation of atomic metallic hydrogen remains an open and unresolved challenge.

Discussion

We have quantified the evolution of optical transparency of diamond anvils operated in DACs. Remarkably, the low energy absorption edge

https://doi.org/10.1038/s41467-026-69533-7

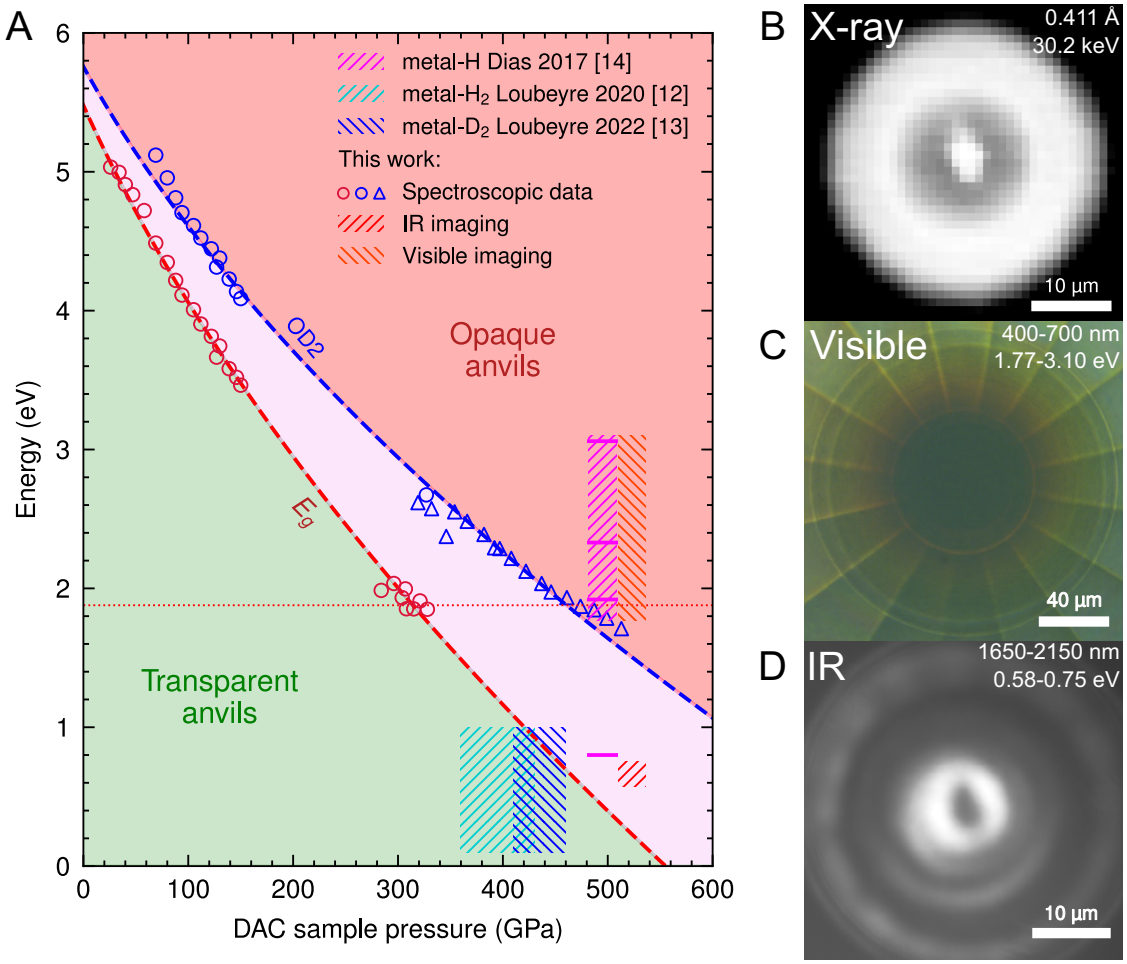

Fig. 4 | Transparency of diamond anvils at multimegabar pressure. A Observed pressure dependence of diamond anvil absorption markers associated with the decrease of its indirect bandgap. The green, purple, and red shaded regions denote the energy–pressure regimes corresponding to transparent, partially absorbing, and opaque anvils, respectively. The dashed areas indicate the regimes where some ultrahigh-pressure experiments have been conducted on hydrogen[12,13,14], along with the present data on Ne. The red dashed horizontal line marks the energy of the 660 nm laser used for Raman excitation. **B** X-ray transmission image of a Ne sample in a DAC at ~523 GPa. **C** Visible light microscopy image of the same sample. The sample is completely obscured by the opaque anvils. **D** Infrared (1650–2150 nm) microscopy image of the same sample. Although anvil transparency is reduced in this spectral range, it remains sufficient to provide optical access to the sample. Joint X-ray, visible and IR imaging has only been performed on the highest pressure sample presented.

behavior is independent of the diamond culet size and shape, analogous to the universality observed in the diamond Raman edge pressure scale, whose calibration is refined in this work. This universality originates from the elastic deformation at the culet surface in contact with the sample. Within a simple mechanics model along the anvil axis, a layer of a few microns in thickness is tetragonally deformed under pressure below the anvil surface, exhibiting an almost constant deviatoric stress anisotropy factor. The minimum indirect bandgap of diamond anvils, tetragonally deformed with a stress anisotropy of 0.6, is then measured to linearly decrease with density and is expected to close when density is reaching 5.4 g/cm^3. Claims in the literature regarding the observation of metallic hydrogen are critically reassessed in light of the present new experimental constraints. Specifically, the reported optical evidence for metal atomic hydrogen around 500 GPa appears to be incompatible with the now well-characterized transparency limits of diamond anvils. Recent advanced calculations place this transition at 577 GPa[38]. Infrared reflectance measurements remain the only viable optical method for characterizing this transition. Using a toroidal-DAC, we show here by compressing Ne that this pressure range is within reach for hydrogen. Although the infrared transparency of the anvils shall be perturbed in the 560 GPa range, it still should allow for the detection of an expected reflectivity jump at the transition. However, should the stability field of metal atomic hydrogen shift beyond 600 GPa, its observation in DACs would likely rely solely on X-ray diagnostics.

Methods

DAC sample preparation

High pressure was generated using LeToullec-type membrane DACs equipped with Boehler-Almax type IIas synthetic diamond anvils obtained from Almax easyLab. Beveled and toroidal anvil shapes were used, as indicated in Supplementary Information Tables 1 and 2. The toroidal shape was machined by focused ion beam machining. The central flat diameter, groove and depth are 24 µm, 80 µm and 4.6 µm, respectively. Rhenium gaskets were used. The neon sample was loaded in the DACs under a pressure of 140 MPa. The sample pressure versus the membrane pressure follows the typical S curve, as illustrated for the highest pressure run in Supplementary Fig. 9. The conversion between the membrane pressure, P_m, and the force on the piston, F, amounts to F [kN] = 0.05 × P_m [bar].

Effective diamond anvil EOS

Quantitative analysis of the optical behavior of diamond anvils with increasing pressure seems to be well linearized by expressing

quantities relative to diamond density. However, the non-hydrostatic nature of the stress field at the diamond anvil tip implies that the relationship between DAC sample pressure and the relevant diamond density is not simply the hydrostatic diamond EOS. To account for this effect, we derived an effective EOS for the diamond at the tip of the diamond anvil from the community-standard IPPS-Ruby2020 hydrostatic diamond EOS[25] combined with a our model of stress anisotropy. This modified EOS, illustrated in Supplementary Fig. 5, is computed from the[25] Vinet EOS with parameters V_0 = 3.4178 cm^3/mol, K_0 = 443.3 GPa, K'_0 = 3.7, corrected considering that the actual average pressure on the anvil tip is $P = P_s(1 + 2\delta)/3$ with δ = 0.6, P_S being the sample pressure. The resulting effective EOS can also be fitted to a Vinet form with parameters K_0 = 604.5 GPa, K'_0 = 3.7.

Anvil absorption model

The intrinsic absorption of the diamond anvils can be approached by a simple model combining different parts of the known behavior of stressed diamond. Qualitatively, the optical path through a loaded diamond anvil is a straight line through a diamond single crystal under a complex stress field. This stress is maximum at the anvil culet, where the normal stress is assumed to be equal to the quasi-hydrostatic pressure within the sample P_s, by continuity. Then it decays through the thickness of the anvil towards its back-face, where the stress is minimal and very close to zero. Along this optical path, light traverses compressed diamond with a pressure gradient, and is progressively absorbed in a spectrally non-uniform way.

To model this effect, we need to combine estimates for three parameters. First, the stress tensor as a function of depth within the stressed anvil $\sigma(z)$. Then, an estimate of the local bandgap evolution with said stress $E_g(\sigma)$. Finally, we need a simple model of the spectral shape of the absorption profile of diamond for a given bandgap value $\alpha(E, E_g)$. These estimates are visually shown in Supplementary Fig. 6. Putting together all of these parameters will confirm that in the case of stressed diamond anvils, the resulting absorption edge at the lowest energy is dominated by the behavior of the thin surface layer at the anvil tip that is submitted to the highest stress, acting like a quasi-uniform slab with an indirect bandgap varying with pressure.

Regarding the stress tensor evolution within the depth of the loaded anvil, this is a complex problem that has been approached many times in past studies. However, we believe that for the purpose of this work, we can apply a simple elasticity model from ref. 29, which has also previously been used in the work of ref. 27. Considering a semi-infinite anvil with applied load q on a disk of radius a, the normal stress field as a function of depth z can be derived as :

$$\sigma_z(z) = q\left[1 - \frac{z^3}{(a^2+z^2)^{3/2}}\right]. \quad (1)$$

In our case, we will consider that load is equal to the hydrostatic pressure at the sample interface $q = P_s$, applied over the area of the disk formed by the culet of the anvil. This gives rise to a stress profile that decays with depth z relative to the the anvil surface, after a small slab of quasi-uniform stress. Notably, this profile does not depend on the elastic properties of the material considered, and the characteristic dimensions of the resulting profile are determined by the disk radius, or culet size in our case. This model may at first seem like an over-simplification, but comparison to our spatially resolved diamond Raman measurements show that it allows a very satisfactory description of physical reality when combined to the usual description of Raman frequency with normal stress[16] (see Fig. 2C), while introducing a minimal number of parameters. The question of transverse stress is much more complex, as it more heavily relies on the elastic properties of diamond, and on the particular massive support geometry of the anvil-gasket assembly. However, following the successful reproduction of the maximum-Raman-signal frequency with anvil depth that we obtained when using[16], we will assume for simplicity that the deviatoric fraction of stress within the anvil is constant, taken as the value measured at the anvil tip.

For the spectral shape of the local absorption edge at a given depth (and thus local stress value), we will simply assume a standard indirect bandgap energy dependence of the absorption coefficient $\alpha(E, E_g)$, of the form:

$$\alpha(E, E_g) = \begin{cases} 0 & \text{for } E < E_g \\ C(E - E_g)^2 & \text{for } E \geq E_g \end{cases} \quad (2)$$

where E is the photon energy, and C is a constant giving the steepness of the absorption edge. Note that we only consider here the absorption due to the diamond's indirect bandgap (no higher energy contribution from the direct gap), and that absorption coefficient values will be limited to a saturation maximum value α_{max} to avoid nonphysical divergences of the quadratic edge (this value only matters for the description of the high energy-high absorbance regime that we are not considering here for the determination of the lowest bandgap).

The bandgap evolution with normal stress will be adjusted to our experimental observation, and taken to be linear in diamond density. Note that the conclusion that the shape of the total absorption edge is consistent with a simple indirect bandgap is essentially independent of the exact shape of $E_g(\sigma)$, as long as it is monotonously decreasing.

Bringing all of these assumptions together, one can estimate the total anvil absorption profile from the following reasoning. At a given sample pressure, we estimate the stress profile within the anvil from P_s and culet radius a. At each depth, we estimate the local absorption coefficient as a function of local gap value, and photon energy. Finally, we numerically sum the contribution throughout the anvil thickness to get an integrated absorbance profile $A(P_s, E, a) = \int_{anvil}\alpha(z, P_s, a, E)\,dz$. Results of this procedure are shown in Supplementary Fig. 6.

Applying parameters relevant to our experimental conditions, the resulting profiles do confirm our observations. In spite of the significant pressure gradient within the bulk of the anvil, the behavior of the absorption profile at low energy is dominated by the absorption of a slab of quasi-uniformly stressed diamond.

Reporting summary

Further information on research design is available in the Nature Portfolio Reporting Summary linked to this article.

Data availability

Source data for all figures are provided with this paper. Raw data and code for this study have been deposited to Zenodo and are accessible with https://doi.org/10.5281/zenodo.18350936 (see ref. 39). Source data are provided with this paper.

References

1. Bassett, W. A. Diamond anvil cell, 50th birthday. *High. Press. Res.* **29**, 163–186 (2009).
2. Hilberer, A. et al. Enabling quantum sensing under extreme pressure: nitrogen-vacancy magnetometry up to 130 GPa. *Phys. Rev. B* **107**, L220102 (2023).
3. Li, B. et al. Diamond anvil cell behavior up to 4 Mbar. *Proc. Natl. Acad. Sci.* **115**, 1713–1717 (2018).
4. Fratanduono, D. E. et al. Establishing gold and platinum standards to 1 terapascal using shockless compression. *Science* **372**, 1063–1068 (2021).
5. Lazicki, A. et al. Metastability of diamond ramp-compressed to 2 terapascals. *Nature* **589**, 532–535 (2021).

6. Dewaele, A., Loubeyre, P., Occelli, F., Marie, O. & Mezouar, M. Toroidal diamond anvil cell for detailed measurements under extreme static pressures. *Nat. Commun.* **9**, 2913 (2018).
7. Dubrovinskaia, N. et al. Terapascal static pressure generation with ultrahigh yield strength nanodiamond. *Sci. Adv.* **2**, e1600341 (2016).
8. Ashcroft, N. W. Metallic hydrogen: a high-temperature superconductor? *Phys. Rev. Lett.* **21**, 1748–1749 (1968).
9. Myung, C. W., Hirshberg, B. & Parrinello, M. Prediction of a supersolid phase in high-pressure deuterium. *Phys. Rev. Lett.* **128**, 045301 (2022).
10. Babaev, E., Sudbø, A. & Ashcroft, N. W. Observability of a projected new state of matter: a metallic superfluid. *Phys. Rev. Lett.* **95**, 105301 (2005).
11. Eremets, M. I., Drozdov, A. P., Kong, P. P. & Wang, H. Semimetallic molecular hydrogen at pressure above 350 GPa. *Nat. Phys.* **15**, 1246–1249 (2019).
12. Loubeyre, P., Occelli, F. & Dumas, P. Synchrotron infrared spectroscopic evidence of the probable transition to metal hydrogen. *Nature* **577**, 631–635 (2020).
13. Loubeyre, P., Occelli, F. & Dumas, P. Compression of D 2 to 460 GPa and isotopic effects in the path to metal hydrogen. *Phys. Rev. Lett.* **129**, 035501 (2022).
14. Dias, R. P. & Silvera, I. F. Observation of the Wigner-Huntington transition to metallic hydrogen. *Science* **355**, 715–718 (2017).
15. Geng, H. Y. Public debate on metallic hydrogen to boost high pressure research. *Matter Radiat. Extrem.* **2**, 275–277 (2017).
16. Akahama, Y. & Kawamura, H. Pressure calibration of diamond anvil Raman gauge to 310GPa. *J. Appl. Phys.* **100**, 043516 (2006).
17. Akahama, Y. & Kawamura, H. Pressure calibration of diamond anvil Raman gauge to 410 GPa. *J. Phys. Conf. Ser.* **215**, 012195 (2010).
18. Eremets, M. I. et al. Universal diamond edge Raman scale to 0.5 terapascal and implications for the metallization of hydrogen. *Nat. Commun.* **14**, 907 (2023).
19. Mao, H. K. & Hemley, R. J. Optical transitions in diamond at ultrahigh pressures. *Nature* **351**, 721–724 (1991).
20. Ruoff, A. L., Luo, H. & Vohra, Y. K. The closing diamond anvil optical window in multimegabar research. *J. Appl. Phys.* **69**, 6413–6416 (1991).
21. Surh, M. P., Louie, S. G. & Cohen, M. L. Band gaps of diamond under anisotropic stress. *Phys. Rev. B* **45**, 8239–8247 (1992).
22. Onodera, A. et al. Pressure dependence of the optical-absorption edge of diamond. *Phys. Rev. B* **44**, 12176–12179 (1991).
23. Trojan, I. A., Eremets, M. I., Korolik, M. Y. U., Struzhkin, V. V. & Utjuzh, A. N. Fundamental gap of diamond under hydrostatic pressure. *Jpn. J. Appl. Phys.* **32**, 282 (1993).
24. Tang, J. et al. Metallization and positive pressure dependency of bandgap in solid neon. *J. Chem. Phys.* **150**, 111103 (2019).
25. Shen, G. et al. Toward an international practical pressure scale: a proposal for an IPPS ruby gauge (IPPS-Ruby2020). *High. Press. Res.* **40**, 299–314 (2020).
26. Mohammed Idris Bakhit, A., Mutisya, S. & Scandolo, S. Raman frequencies of diamond under non-hydrostatic pressure. *Appl. Phys. Lett.* **119**, 211902 (2021).
27. Ruoff, A. L. & Luo, H. Pressure strengthening: a possible route to obtaining 9 Mbar and metallic diamonds. *J. Appl. Phys.* **70**, 2066–2070 (1991).
28. Akahama, Y. & Kawamura, H. Raman study on the stress state of [111] diamond anvils at multimegabar pressure. *J. Appl. Phys.* **98**, 083523 (2005).
29. Timoshenko, S. P. & Goodier, J. N. *Theory of Elasticity* (McGraw-Hill Book Company Inc., 1951).
30. Lee, S. K. et al. Imaging of the electronic bonding of diamond at pressures up to 2 million atmospheres. *Sci. Adv.* **9**, eadg4159 (2023).
31. Clark, C., Dean, P. J. & Harris, P. V. Intrinsic edge absorption in diamond. *Proc. R. Soc. Lond. Ser. A. Math. Phys. Sci.* **277**, 312–329 (1964).
32. Cheng, L., Zhu, S., Ouyang, X. & Zheng, W. Bandgap evolution of diamond. *Diam. Relat. Mater.* **132**, 109638 (2023).
33. Asaumi, K., Mori, T. & Kondo, Y. Effect of very high pressure on the optical absorption edge in solid Xe and its implication for metallization. *Phys. Rev. Lett.* **49**, 837–840 (1982).
34. Pascarelli, S. et al. Materials under extreme conditions using large X-ray facilities. *Nat. Rev. Methods Prim.* **3**, 82 (2023).
35. Ji, C. et al. Ultrahigh-pressure crystallographic passage towards metallic hydrogen. *Nature* **641**, 904–909 (2025).
36. Goncharov, A. F. & Struzhkin, V. V. Comment on "Observation of the Wigner-Huntington transition to metallic hydrogen". *Science* **357**, eaam9736 (2017).
37. Liu, X. D., Dalladay-Simpson, P., Howie, R. T., Li, B. & Gregoryanz, E. Comment on "Observation of the Wigner-Huntington transition to metallic hydrogen". *Science* **357**, eaan2286 (2017).
38. Monacelli, L., Casula, M., Nakano, K., Sorella, S. & Mauri, F. Quantum phase diagram of high-pressure hydrogen. *Nat. Phys.* **19**, 845–850 (2023).
39. Hilberer, A. et al. Source data for: Spectroscopic limits of diamond anvils to 520 GPa and projected bandgap closure. *Zenodo* https://doi.org/10.5281/zenodo.18350936 (2026).

Acknowledgements

We acknowledge European Synchrotron Radiation Facility (ESRF) access under proposal HC-4884 for X-ray diffraction data on gold and Ne, and we thank M. Mezouar for assistance on the ID27 beamline and for helpful discussions. We acknowledge SOLEIL Synchrotron access under proposal 20241170 and thank F. Jamme for providing access and help with the DISCO UV beamline. We thank G. Geneste for valuable discussions.

Author contributions

P.L. and P.D. designed the project. P.L. and F.O. prepared the DACs. R.A. FIB-machined the toroidal anvils and gasket holes. P.D. and C.P. performed the UV absorption measurements. P.D. and A.H. performed the visible-IR absorption measurements. G.W., F.O., A.H., and P.L. performed the XRD measurements. A.H. and F.O. performed the Raman measurements. A.H., C.P., P.D., and P.L. analyzed the absorption data. G.W. and A.H. analyzed the XRD data. A.H. and P.L. wrote the draft. All authors discussed the data and revised the manuscript.

Competing interests

The authors declare no competing interests.

Additional information

Supplementary information The online version contains supplementary material available at https://doi.org/10.1038/s41467-026-69533-7.

Correspondence and requests for materials should be addressed to A. Hilberer or P. Loubeyre.

Peer review information *Nature Communications* thanks the anonymous reviewers for their contribution to the peer review of this work. A peer review file is available.